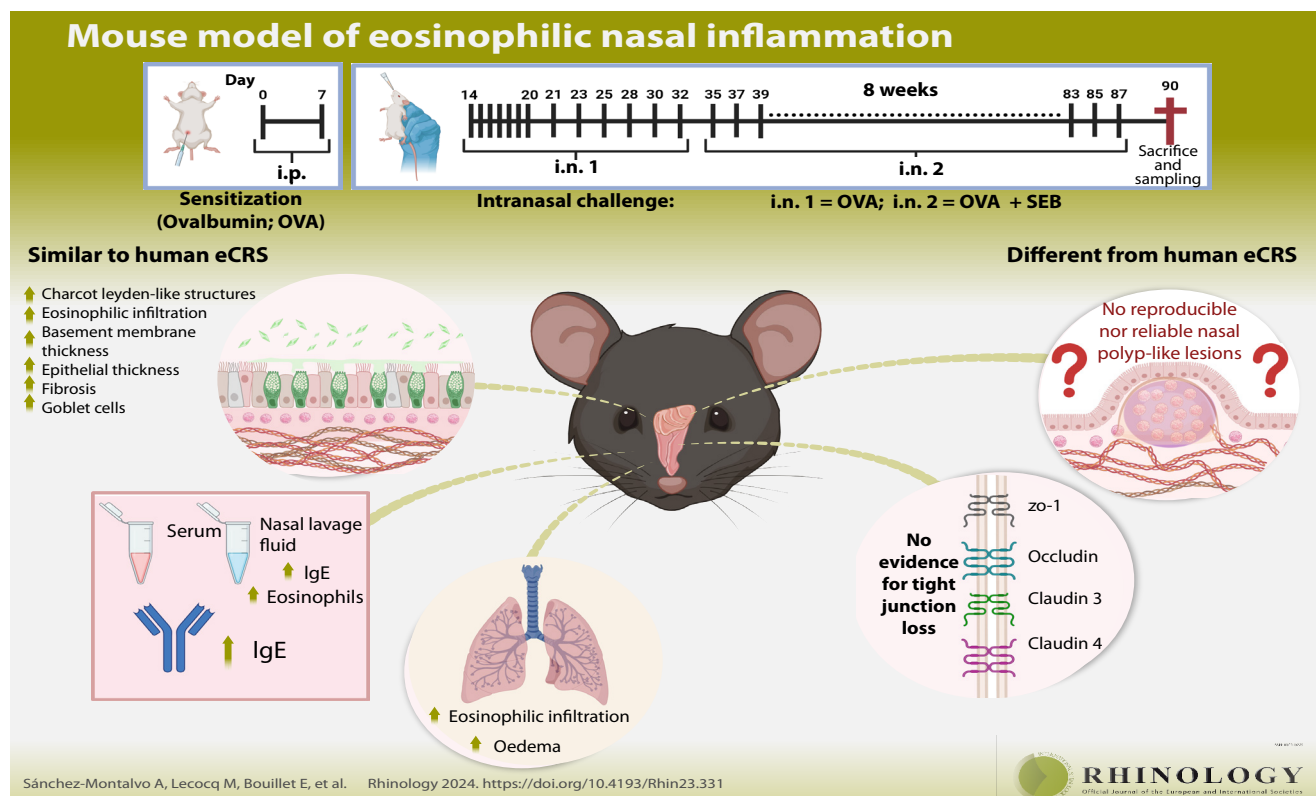


Validation and shortcomings of the most common mouse model of chronic rhinosinusitis with nasal polyps

Alba Sánchez-Montalvo^{1,2}, Marylène Lecocq¹, Elise Bouillet¹, Brecht Steelant²,
Sophie Gohy^{1,3,4}, Antoine Froidure^{1,3}, Dominique Bullens^{2,5}, Charles Pilette^{1,3},
Valérie Hox^{1,6}

Rhinology 62: 4, 446 - 456, 2024

<https://doi.org/10.4193/Rhin23.331>



Abstract

Background: Chronic rhinosinusitis (CRS) is a highly prevalent airway disease worldwide. Whereas eosinophilic CRS with nasal polyps (eCRSwNP) represents its most severe phenotype, pathogenic mechanisms remain poorly understood despite a wide spectrum of in vitro and in vivo experimental models. A mouse model of experimental ovalbumin (OVA)-induced airway allergy with coadministration of *Staphylococcus aureus* enterotoxin B (SEB) has been widely used to study eosinophilic eCRSwNP. This study revisits the features of this model and its suitability for studying eCRS. **Methodology:** We implemented the most used eCRSwNP mouse model based on OVA+SEB intranasal challenges. Readouts including inflammatory features by (immuno)histology of the sinonasal epithelium (NP formation, eosinophils, epithelial and basement membrane thickness, fibrosis, goblet cells, Charcot-Leyden crystals (CLC)-like, tight junctions) and IgE production by enzyme-linked immunosorbent assay (ELISA), were compared to features of the corresponding human disease. **Results:** The OVA+SEB model induced eosinophilic inflammation of upper and lower airways, with epithelial and basement membrane thickening, goblet cell hyperplasia and subepithelial fibrosis in the sinuses, along increased IgE production. Except local IgE in nasal lavage (NL), which was only increased in OVA+SEB group, all other features did not differ between OVA and OVA+SEB groups. Macro- or microscopic NP were not detected. **Conclusions:** With the notable exception of local IgE production, the addition of SEB did not induce additional inflammatory or structural change in the sinuses from mice exposed to and challenged with OVA. This model might represent a model for severe upper airway allergy rather than a specific model of human eCRSwNP.

Key words: chronic rhinosinusitis, maxillary sinus, nasal polyps, rhinitis

Introduction

Chronic rhinosinusitis (CRS) is one of the most common upper airway inflammatory diseases in the Western world, with a prevalence of 11%⁽¹⁾. CRS may severely impair patients' quality of life, leading to a significant socio-economic burden⁽²⁾. In the most recent guidelines, CRS is classified according to its inflammatory subtype: Type 2 (T2) inflammation, characterized by the canonical T helper (h) 2 inflammatory pathways; and non-T2 inflammation, a more heterogeneous group characterized by the presence of Th1/Th17/Th22 cytokines⁽³⁾. In the Western world, patients with a T2 profile often present with the formation of nasal polyps (NP) arising from the paranasal sinuses and protruding into the nasal cavities⁽⁴⁾. Patients suffering from eCRS with NP (eCRSwNP) suffer from more severe symptoms and experience increased recurrence after surgery compared to non-T2 patients⁽³⁾. Moreover, it has been described that around 22-40% of patients with eCRS present with asthma, fitting the united airways hypothesis⁽⁵⁾.

Although many scientific advancements have helped unraveling disease mechanisms of T2 eCRS in recent years⁽⁶⁻⁹⁾, its exact pathophysiology and driving triggers for NP formation remain elusive. One of the best-studied disease-modifying factors is increased sinonasal colonization with *Staphylococcus aureus* and the link between its enterotoxins and CRSwNP. Especially, *Staphylococcus enterotoxin B* (SEB) plays a role as a superantigen but can also elicit several direct harmful effects on the respiratory mucosa⁽¹⁰⁻¹⁴⁾. Another feature that has arisen as a key driver for CRSwNP is the loss of the epithelial barrier function formed by e.g. junctional complexes^(15,16), which can also be affected by SEB⁽¹⁷⁾.

Because of the IgE-mediated eosinophilic T2 inflammation seen in most CRSwNP patients, it was initially thought that IgE-mediated allergy was the inciting factor for this disease. Therefore, the link with allergic rhinitis (AR) has been extensively studied⁽¹⁸⁾. However, it has become clear that not all patients with CRSwNP suffer from allergy and, to date, there's no conclusive evidence linking allergy to CRS. Some specific phenotypes of CRSwNP such as allergic fungal rhinosinusitis (AFRS) and the more recently described central compartment atopic disease (CCAD) seem to be more related to allergy. However, in other CRS phenotypes the prevalence of AR does not appear to be higher than in the general population⁽¹⁹⁾. Additionally, AR is a very prevalent disease that shows a significant overlap in symptomatology and histopathology with CRS⁽³⁾.

Studying the pathophysiology of human disease is often limited due to the heterogeneity of patient population, which could be partially solved by the availability of a suitable animal model. In the past decades, murine models have emerged as useful

tools to study immunological pathways in respiratory diseases such as asthma and AR^(20,21). Despite the differences between humans and mice, their airway organization and immunological responses are comparable⁽²²⁾. In 2011, a mouse model of eCRS was described by Kim⁽²³⁾. This model was based on the induction of experimental airway allergy followed by nasal exposure to SEB⁽²³⁾. As a result, mice developed an eosinophilic influx at the sinus epithelium, characterized by general features of T2 inflammation. However, the major drawback of this model was the lack of development of macroscopic NPs, as seen in humans. Despite that, this mouse model has been widely used in a growing number of publications investigating the mechanisms of human eCRSwNP⁽²⁴⁾.

In this study, we aimed to evaluate the classical inflammatory features of this mouse model in a critical way. We searched whether the addition of SEB truly added value to the classical AR mouse and compared its features to those of human eCRSwNP. This document describes our experiences with this widely used eCRS model. We discuss the different issues related to it and from which researchers in this field may benefit when interpreting results and the gaps that maintain for the establishment of a more adequate mouse model for eCRSwNP.

Materials and methods

More detailed information can be found in supplementary files.

Experimental procedure to induce an experimental eosinophilic CRS in mice

Animal model

C57BL/6NRJ female mice were divided into four groups (n=4-10/group): control, SEB, OVA, and OVA+SEB (Figure 1). Mice were sensitized with an intraperitoneal (i.p.) injection of ovalbumin/aluminum on days 0 and 7. This was followed by one week of daily intranasal (i.n.) challenges with 6% OVA. These i.n. challenges were then continued three times a week for eight weeks. Mice planned to develop eCRS, received, in addition to i.n. OVA-challenges, a second i.n. challenge with SEB during the last eight weeks. All animal experiments were performed in compliance with the ethical committee guidelines and approved under reference code 2018/UCL/MD/42.

Sacrifice and sampling

Three days after the final challenge, mice were euthanized and blood was drawn for serum collection. Nasal lavage (NL) fluid and Bronchoalveolar Lavage (BAL) were collected and centrifuged to obtain cytopins and supernatant. Lungs were rinsed and lung lobes were fixed in formaldehyde 4% for histology. Skulls were harvested by decapitation and skin, soft tissues and inferior mandibula were removed. They were fixed in formaldehyde 4% and decalcified in OsteoraTM (RAL Diagnostics) for five

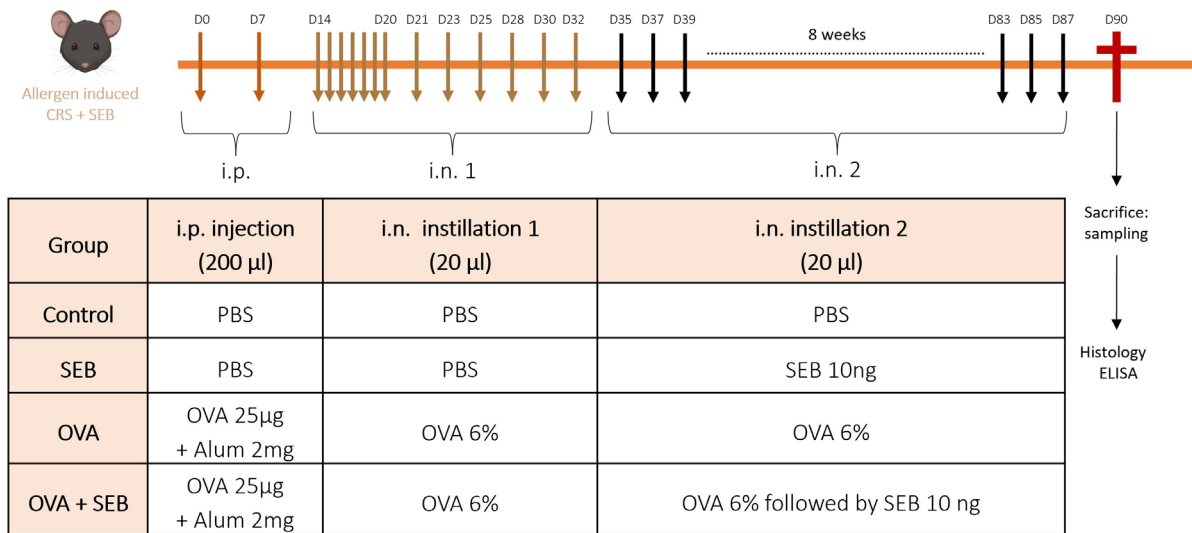


Figure 1. Experimental protocol for the induction of eCRS based on the original published model (23). OVA: ovalbumin; SEB: *Staphylococcus aureus* enterotoxin B; Alum: aluminum.

days. Decalcified skulls and lungs were dehydrated and treated according to standard paraffin-embedding procedures and cut into 4µm sections.

Histopathologic analysis of the paranasal sinus epithelium

Paraffinized 4µm sections of the decalcified skulls were used for histological analysis. To standardize the analysis, three fixed areas from the right and the left maxillary sinus were taken to evaluate histological features (Figure 2). After being stained, all slides were coverslipped and scanned with a Panoramic scan II (3DHistech). Stained skulls were scanned in a randomized way. Microscopic analysis and quantification were performed in a blinded fashion.

To study epithelial integrity and height and formation of NP-like lesions, H&E staining was performed. NP-like lesions were defined similarly to previously published as an edematous projection from the lining of the epithelium to the lumen, filled with eosinophils (23). NP-like lesions were only considered when appearing in three consecutive sections at three consecutive levels of the skull to account for artifacts. Maxillary sinuses, as well as ethmoidal sinuses, olfactory cleft and nasal cavity lining were evaluated for counting NP-like structures. Giemsa staining was performed to evaluate goblet cell hyperplasia and eosinophilic infiltration. Sirius red (SR) staining was performed to measure basement membrane thickness, collagen deposition and to evaluate the presence of CLC-like structures in the nasal and sinus lumen.

Immunohistochemical expression of tight junctions in the sinus epithelium

As primary antibodies, rabbit anti-mouse Claudin 3 (Invitrogen,

34-1700), mouse anti-mouse Claudin 4 (Invitrogen, 32-9400), rabbit anti-mouse occludin (Invitrogen, 71-1500) and mouse anti-ZO1 (Invitrogen, 33-9100) were used. Quantification strategy and TJs staining are available as supplementary material.

Total IgE and cytokine measurements

Serum and NL levels of total IgE were determined by ELISA. Purified mouse IgE (BD Pharmingen 553413) was used as capture antibody, Purified Mouse IgE κ Isotype Control was used to create standards (BD Pharmingen, 557079) and Biotinylated anti-mouse IgE (BD Pharmingen, 553419) was used for detection (detection limit= 2.87ng/ml). Levels of IL-4 and IL-5 were determined in the NL by ELISA following the instructions by the DuoSet® ELISA (R&D systems, detection limit= 62,5 pg/ml for IL-4 and 125 pg/ml for IL-5). Serum samples were diluted 1:25 in PBS-BSA 1% and NL samples were used undiluted.

Histopathologic analysis of the bronchial epithelium

Paraffinized 4µm sections of fixed left lung lobe were stained with Giemsa to evaluate the general state of the bronchial epithelium and eosinophilic infiltration.

Statistical analysis

Analysis was performed with GraphPad Prism version 8.0.0 (GraphPad Software, San Diego, CA, USA). Results are presented as median from each group ± interquartile range (IQR). Statistical differences between experimental groups were evaluated with the Kruskal-Wallis test for comparing multiple groups. A value of p<0.05 was considered significant.

Results

Mice treated with OVA show an eosinophilic inflammation of

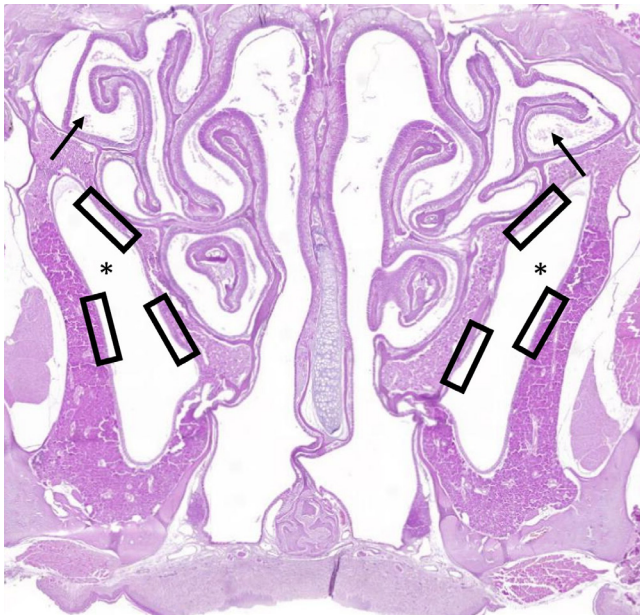


Figure 2. Coronal section of the sinonasal complex of mice showing the maxillary (*) and ethmoidal sinuses (arrow), H&E staining. Rectangles indicate the regions of the maxillary sinuses that were selected in each mouse to evaluate different histological features in a systematic way.

the nose and sinuses

In NL, eosinophils were increased in mice treated with OVA without or with SEB compared to mice receiving PBS ($p < 0.05$ and $p < 0.01$, respectively) (Figure 3A). Neutrophil counts were not different among groups (Figure 3B). At tissue level, sub- and intraepithelial eosinophilic infiltration was increased in mice receiving OVA alone and OVA+SEB compared to those receiving PBS ($p < 0.05$ and $p < 0.001$, respectively) and in mice receiving OVA+SEB compared to SEB alone group ($p < 0.05$) (Figure 3C-D). CLC-like were detected in the sinuses and nasal fossae of all mice treated with OVA, in similar quantities between the OVA and OVA+SEB groups compare to mice treated with PBS and SEB alone (both $p < 0.001$ and both $p < 0.05$ respectively) (Figure 3E-F). No differences were found between OVA and OVA+SEB groups for the above-mentioned parameters.

OVA-treated mice show increased systemic IgE production. The addition of SEB to OVA induces the production of local IgE production

Total serum IgE levels were higher in mice receiving OVA and OVA+SEB compared to mice receiving PBS (both $p < 0.05$). No difference in serum IgE levels was found between the OVA and OVA+SEB groups (Figure 3G). Three of nine mice treated with OVA+SEB showed detectable IgE levels in their NL; all other values were below the detection limit (Figure 3H). IL-4 and IL-5 in the NL were below detection level in the NL of all mice (data not shown).

Mice treated with OVA and OVA+SEB show similar epithelial abnormalities and remodeling at the level of the sinuses

On H&E-stained skulls, the epithelial cell layer of the maxillary sinus was thicker in mice challenged with OVA alone and OVA+SEB compared with mice receiving PBS ($p < 0.01$ and $p < 0.001$, respectively) (Figure 4A-B). Goblet cells were more abundant in mice treated with OVA and OVA+SEB than in mice treated with PBS ($p < 0.05$ and $p < 0.001$) (Figure 4C-D). Also, basement membrane thickening was more pronounced in mice treated with OVA and OVA+SEB compared with mice receiving PBS ($p < 0.05$ and $p < 0.001$, respectively) (Figure 4E-G). Subepithelial fibrosis was higher in the OVA and OVA+SEB groups compared with mice challenged with PBS ($p < 0.01$ and $p < 0.001$, respectively) (Figure 4F-G). At the level of tight junction expression, no differences were seen among the treated groups (Figure 4H; Figures S1, S2). No changes were found between OVA and OVA+SEB groups for the above-mentioned epithelial changes.

In our hands, no NP-like lesions were detected in the maxillary, nasal fossae, or ethmoidal sinuses of mice treated with OVA+SEB, nor in any of the other groups.

Mice treated with OVA and OVA+SEB develop eosinophilic lower airway inflammation

Total inflammatory cell count was higher in the BAL of mice receiving OVA+SEB compared with mice treated with PBS ($p < 0.01$) (Figure 5A). BAL eosinophils were increased in the OVA alone and OVA+SEB groups compared with mice receiving PBS (both $p < 0.05$) (Figure 5B). Neutrophils were higher in mice receiving OVA+SEB group ($p < 0.05$) (Figure 5C). These findings were confirmed by histology, showing general edema, increased basement membrane thickening and peri-bronchial eosinophilic infiltration in the lungs of mice treated with OVA and OVA+SEB (Figure 5D). Moreover, both OVA and OVA+SEB groups showed local production of IgE in the BAL compared with mice challenged with PBS (both $p < 0.05$) (Figure 5E). There was no difference between OVA and OVA+SEB groups for any of the above-mentioned parameters.

Discussion

In this study, we aimed at establishing and critically evaluating one of the most used mouse models to study eCRSwNP disease mechanisms. The model is based on the addition of the superantigen SEB to a mouse model of experimental respiratory allergy, in this case, induced by OVA. In our hands, C57/BL6 mice treated with OVA alone and OVA+SEB showed similar histological sinonasal changes at the maxillary sinuses, such as eosinophilic infiltration, increased epithelial and basement membrane thickening, goblet cell hyperplasia, subepithelial fibrosis and the presence of CLC-like elements. We also detected increased systemic IgE production and inflammatory changes in lower airways.

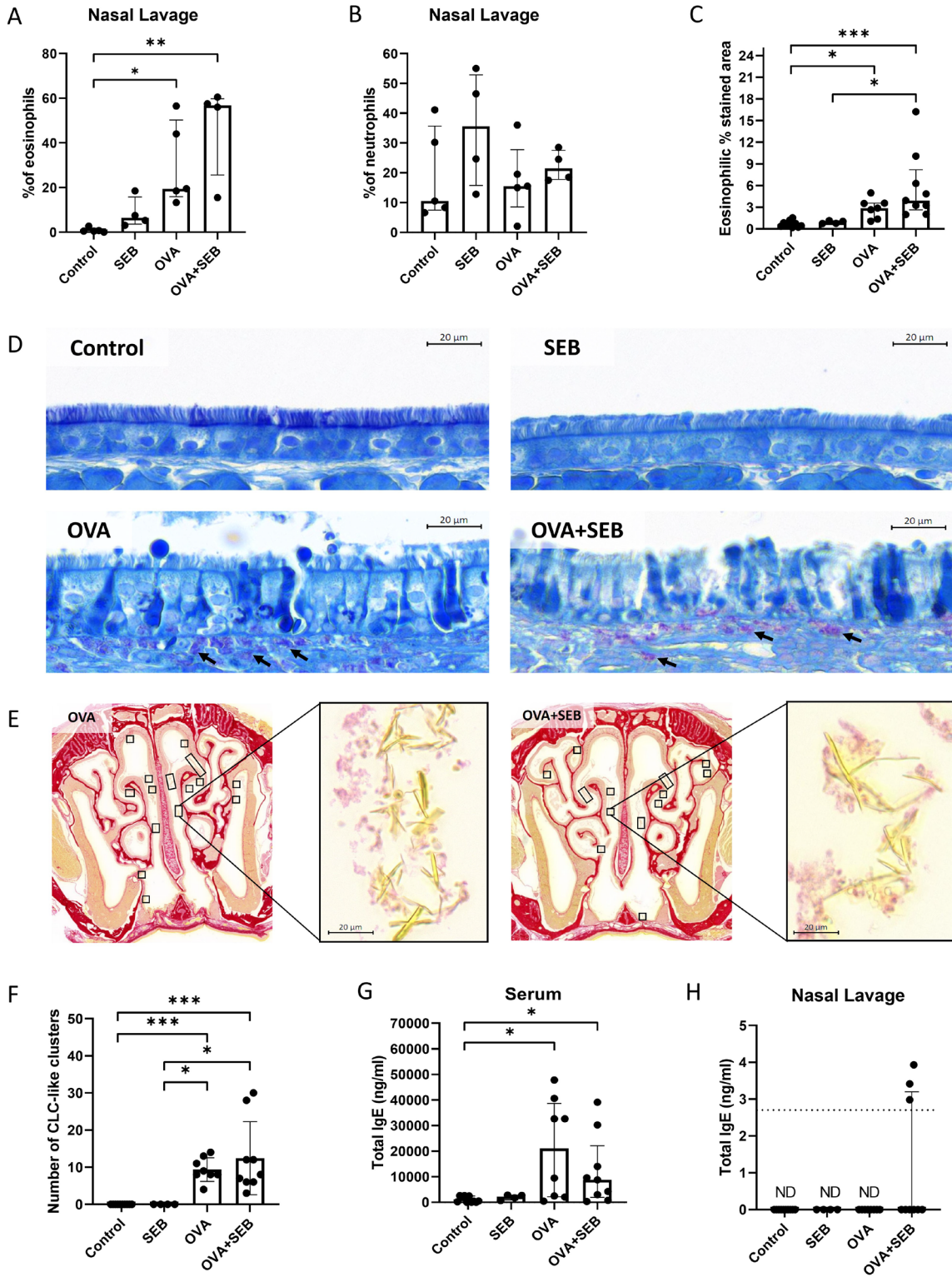


Figure 3. T2 inflammatory markers in an experimental mouse model of eCRS. A) Eosinophils percentage of total inflammatory cells recovered from the NL. B) Neutrophils percentage of total inflammatory cells recovered from the NL. Graph depicts median (\pm IQR). C) Eosinophilic infiltration quantification. Graph depicts median (\pm IQR) of 6 measurements per mouse. Quantification was performed by using QuPath⁽⁴⁸⁾. D) representative Giemsa-stained sections of the epithelial layer from maxillary sinuses. Eosinophils infiltrating the subepithelial space are stained pink-purple (arrow). E) representative CLC-like structures found in OVA (left) and OVA+SEB (right) groups, Sirius Red staining. F) counting of the number of clusters of CLC-like structures Graph depicts median (\pm IQR). G) total IgE levels in serum. Graph depicts median (\pm IQR). H) total IgE levels in NL. Graph depicts median (\pm IQR). ELISA detection limit was 2.87 ng/ml. Kruskal-Wallis test: * $p < 0.05$; ** $p < 0.01$; *** $p < 0.001$. ND: non-detectable. Scale bar= 20 μ m.

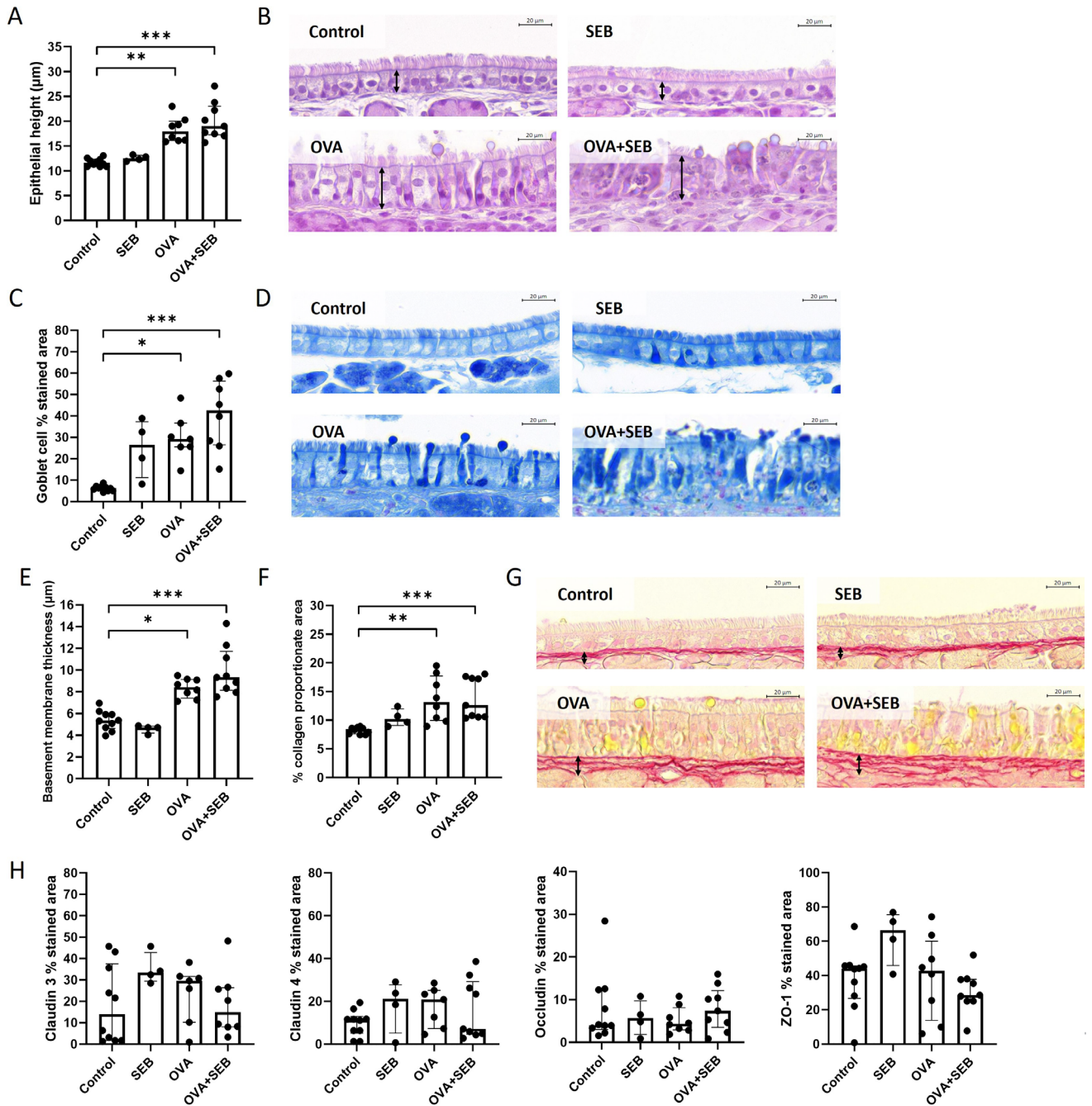


Figure 4. Airway epithelial remodeling in experimental eCRS. A) epithelial thickness measurements quantification. Graph depicts median (\pm IQR) of 24 measurements per mouse performed by using Cytomine⁽⁴⁹⁾. B) representative H&E-stained sections of the epithelial layer from maxillary sinuses. Arrows indicate how epithelial height was measured. C) goblet cell quantification. Graph depicts median (\pm IQR) of 6 measurements per mouse. Quantification was performed by using QuPath⁽⁴⁸⁾. D) representative Giemsa-stained sections of the epithelial layer from maxillary sinuses. Goblet cells are stained in dark blue. E) basement membrane thickness measurements quantification. Graph depicts median (\pm IQR) of 24 measurements per mouse performed by using Cytomine⁽⁴⁹⁾. F) collagen deposition quantification. Graph depicts median (\pm IQR) of 6 measurements per mouse. Quantification was performed by using ImageJ, as described by Courtoy et al.⁽⁵⁰⁾. G) representative SR-stained sections of the epithelial layer from maxillary sinuses. Arrows indicate how basement membrane measurement was performed. H) tight junctions' expression and quantification. Graphs depict median (\pm IQR) of 6 measurements per mouse. Quantification was performed by using QuPath⁽⁴⁸⁾. Kruskal-Wallis test: * $p < 0.05$; ** $p < 0.01$; *** $p < 0.001$. ND: non-detectable. Scale bar = 20 μm .

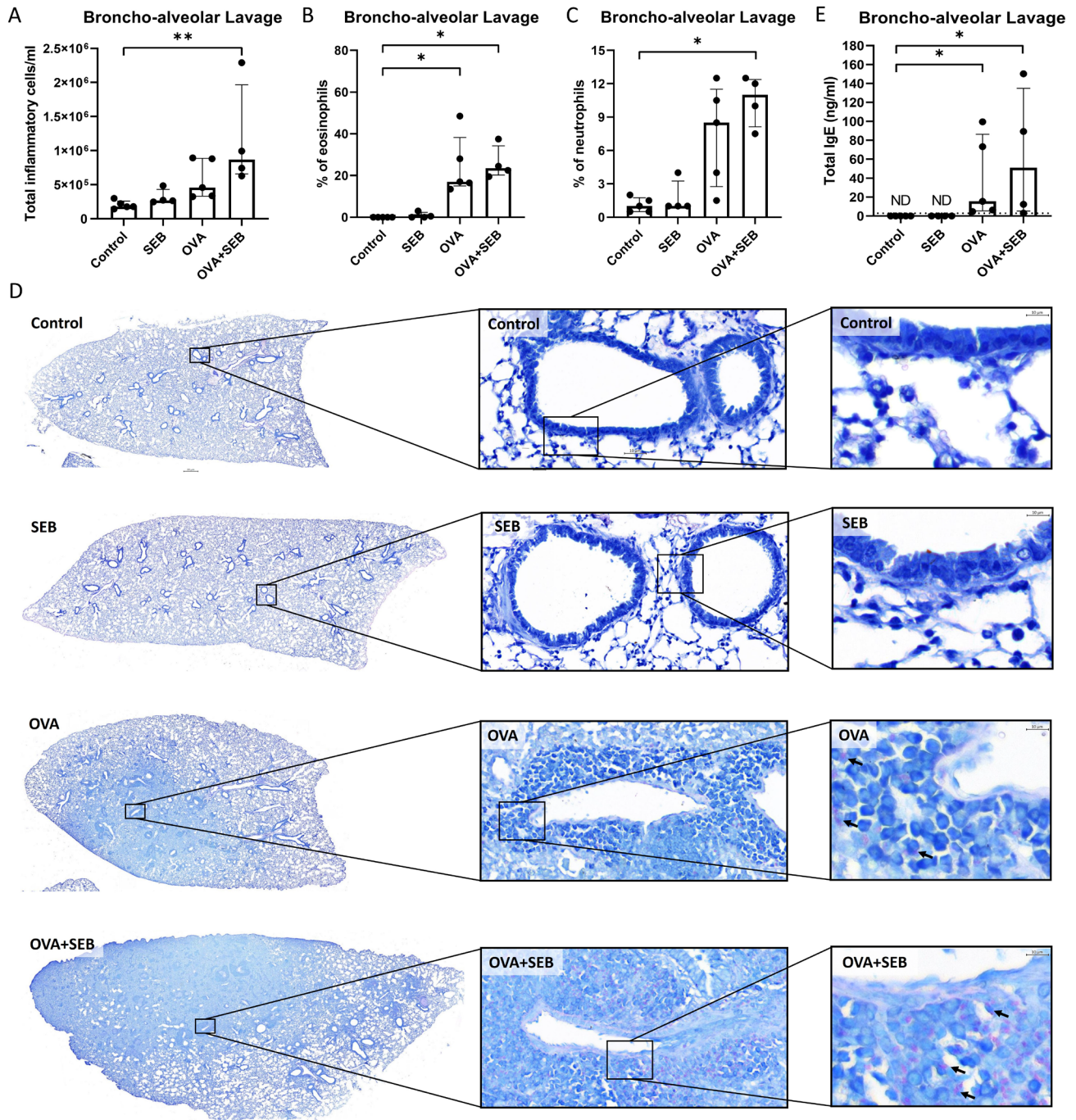


Figure 5. Inflammatory features in the lower airways in experimental eCRS. A-C) Inflammatory cell count in BAL: A) total inflammatory cells, B) eosinophils, C) neutrophils. Graphs depict median (\pm IQR). D) Overview of Giemsa-stained lung lobes in a mouse model of experimental eosinophilic CRS. Eosinophils infiltrating the subepithelial space are stained pink (arrow). E) Total IgE levels in BAL. ELISA detection limit was 2.87 ng/ml. Kruskal-Wallis test: * $p < 0.05$; ** $p < 0.01$. Scale bar, 10 μ m. BAL: bronchoalveolar lavage. ND: non-detectable.

The only difference between mice receiving OVA and OVA+SEB, in our hands, was the induction of local nasal IgE in OVA+SEB mice. No NP or NP-like lesions were detected in sinuses of OVA+SEB mice in our model.

Eosinophilic infiltration and IgE production are typical features

of T2 diseases such as AR and eCRS_{NP}. B-cells are triggered to produce IgE antibodies in a T2 environment that is induced by exposure to allergens or other microbial/environmental antigens⁽²⁵⁾. Increased levels of serum IgE are found in all AR patients, and some eCRS_{NP} patients. eCRS_{NP} patients typically show increased levels of local, polyclonal IgE in their

NP tissue, which is believed to be the result of the superantigen effect of *Staphylococcal aureus* enterotoxins on the local B-cells⁽²⁵⁾. Eosinophils are attracted and activated by the T2 cytokine IL-5, which is elevated in both AR and eCRSwNP patients⁽²⁶⁾. The action of these cells is then responsible for causing a chronic inflammatory state in the sinonasal mucosa, leading to general inflammatory characteristics such as goblet cell hyperplasia, basement membrane thickening and fibrosis being features of chronic inflammation. Why CRSwNP patients develop a more severe disease at the level of the sinus mucosa with the formation of large nasal polyps that can protrude to the nasal cavity, is still not well understood.

For decades, researchers have been trying to elucidate the trigger for NP formation in CRSwNP, which included the search for a relevant mouse model. Most of these mouse models have been based on a respiratory allergy model to induce the required T2 response and allergens used range from the food allergen OVA to house dust mite and fungal allergens^(27,28). Because of the belief that the local polyclonal IgE production upon exposure to SEB could contribute to NP formation, a South Korean group decided to expose OVA-allergic mice to SEB to develop an eCRSwNP mouse model⁽²³⁾. Unfortunately, this model did not lead to the formation of macroscopical NP, as seen in human CRSwNP. However, they do describe the presence of a few microscopic “NP-like lesions”, defined as eosinophilic protrusions of the epithelium involving micro cysts, being limited to one to four lesions per mouse. Most of these lesions were found at the level of the nasal passage (septum and turbinates) rather than in the paranasal sinuses⁽²³⁾. Later, only a few papers addressed these microscopic NP-like structures in a reliable way. Graphs showing the number of NP-like lesions are often not accompanied by histological pictures of the lesions and if they are, they are mostly located outside the paranasal sinuses (septum and nasal floor) and can easily be confused with artefacts⁽²⁴⁾.

In our study, we were not able to detect any of these NP-like lesions in either of the experiments at the level of the maxillary and ethmoidal sinuses, olfactory cleft or nasal cavity lining. It is important to mention that we used the modified version of Kim’s initial protocol (using 10ng of SEB and a slightly shorter challenge phase). However, this is the protocol that has been used in most of the articles reporting on this mouse model⁽²⁴⁾. The absence of NP-like lesions in our hands could be explained by the use of C57BL/6 mice, which are genetically less prone to develop severe T2 disease. However, we observed a severe eosinophilic tissue inflammation with the presence of Charcot-Leyden-type crystals. It does raise the question whether these NP-like structures are really similar to what is seen in human eCRS.

One of the explanations for the above-mentioned limitation might be that mice may not be able to develop NP due to anatomical differences between humans and mice or differences in the local mucosal immune system⁽²²⁾. Another explanation could be that the current experimental protocol is not ideal for developing severe sinus inflammation with NP formation. One of the issues is that mouse models are limited in time and chronicity levels, since the ones observed in human eCRS cannot be reached in mice. There is also the possibility that allergic inflammation and SEB are not the (only) required mediators to develop CRSwNP or that the local inflammation induced might not be sufficiently severe to disrupt the epithelium in a way prompting NP formation. An old paper from Karolinska showed in a rabbit model of surgically induced infectious maxillary sinusitis that larger edematous NPs were formed in areas of severe epithelial desquamation, subepithelial edema and inflammatory cell influx. They showed that epithelial dedifferentiation and cell migration led to the formation of subepithelial microcavities and the formation of polyp stalks evolving to larger NPs⁽²⁹⁾. Interestingly, in our study, we did not show a loss of tight junctions in the sinus epithelium of mice treated with OVA+SEB. This suggests a lack of mucosal barrier defect in contrast to what is seen in human CRSwNP⁽³⁰⁾, being one of the potential key triggers of NP formation.

Our study has several limitations, such as the fact that we stuck to a single mouse strain and allergen. However, we followed a consequent and reproducible methodology, which we feel is often lacking in other papers describing this model. The quantification of inflammatory tissue changes was performed in a consistent way sticking to 6 well-defined areas in the maxillary sinus. We avoided looking at ethmoidal sinuses because of their density in mice, leading to artifacts in histological staining. Unlike most other studies, we decided to not consider the septum and lateral nasal wall, since we were evaluating sinus disease and not rhinitis. Additionally, in contrast to other papers, we included all experimental groups, including mice treated with OVA and SEB alone.

This led us to one of the pivotal observations of this study – the absence of differences between mice treated with OVA alone and OVA+SEB. Interestingly, apart from nasal IgE levels, we did not find significant differences in inflammatory features between mice treated with OVA alone (corresponding to a chronic AR mouse model) and those additionally receiving SEB. Most of the studies using this mouse model to study disease mechanisms of eCRSwNP only compared the OVA+SEB group with a control group. The initial publication by Kim showed an OVA alone group with a significant increase in local eosinophils, IL-5 and eotaxin levels between OVA and OVA+SEB groups⁽²³⁾, which we could not detect (eotaxin not measured). Their observed dif-

Table 1. Inflammatory features of the OVA/SEB mouse model in comparison to human eCRS and AR.

Inflammatory features	Murine model of eCRS	Human AR	Human eCRSwNP
Eosinophilic infiltration	✓	✓	✓
IgE production	✓	✓	✓
Epithelial disruption and thickening	✓	✓	✓
Goblet cell hyperplasia	✓	✓	✓
Basement membrane thickening	✓	✓	✓
Type 2 cytokine production	✓	✓	✓
Decreased tight junction expression	✗	✓	✓
Edema with NP formation	✗	✗	✓
United airway disease	✓	✓	✓

ferences, however, can be attributed to SEB having an adjuvant effect on allergic sensitization, as has been shown previously in a mouse model of OVA-induced AR (31). Furthermore, their use of BALB/c mice, instead of C57BL/6NRJ mice in our protocol, could explain differences detected in their study (32–34).

Although this is a mouse model of eCRS, we question whether it is a suitable model to study eCRSwNP. All inflammatory findings described are features of both human eCRS and AR, and the most robust histopathological difference between the two diseases is the formation of large polyps in the sinus, lacking in our mouse model (Table 1). In humans, up to date, there are no other histopathological features distinguishing AR from eCRS and diagnosis of eCRS is based on symptoms and radiology which are currently not measurable in mice in a reliable way.

Although biopsy studies are lacking, there is evidence that patients with AR also show T2 inflammation in their sinuses (35) and around 40% of eCRSwNP also suffer from AR (18). Yet, despite overlap in symptomatology and T2 inflammatory profile, AR and eCRSwNP are two different disease entities requiring different treatment strategies (8). Also, studies investigating the role of allergy as a contributing factor to eCRSwNP show contradictory results (19) and differences exist between the two diseases such as eosinophil activation levels, local remodeling leading to NP formation and presence of neutrophils (36). There is growing recognition that even T2 CRSwNP population consists of a heterogeneous patient group where different disease mechanisms are playing. Notably, it has been suggested that the recently described CRS endotype “CCAD” might be more related to IgE-mediated allergic phenomena than other types of T2 eCRSwNP, such as seen in severe asthma or Samter’s triad (37). We can thus

speculate that the OVA+SEB mouse model might be a proper tool to study disease mechanisms of CCAD, but less those of other eCRSwNP endotypes. The spatial distribution of the NP-like lesions shown in mice by other authors, mostly found in the nasal fossa rather than in the sinuses (23,38–44), supports the theory of a more CCAD-like phenotype of the mouse model (3).

Finally, we want to highlight that we detected T2-related inflammatory changes in the lower airways of mice treated with OVA and OVA+SEB, resembling features associated with allergic asthma. These findings manifested even though the nasal installation volumes were too small to reach the lower airways (45,46). Although we did not perform any functional bronchial testing, this emphasizes the importance of the robust connection between upper and lower airways, mirroring the observed interplay in human AR and eCRS (47).

Conclusion

By critically evaluating the most used mouse model of eCRSwNP, we could not find any distinct immune-inflammatory or structural changes between OVA and OVA+SEB challenges, except local IgE production. No nasal polyps were detected, which currently represents a unique phenotypic trait for human CRSwNP. This study thus questions whether the OVA+SEB model represents a model for severe upper airway allergy rather than a model for human CRSwNP, and advocates for further research in the field to better mimic the corresponding human diseases.

Authorship contribution

ASM: data collection, data analysis, experimental design, intellectual analysis, writing and reviewing of the manuscript. ML: data collection, data analysis and reviewing of the manuscript. EB: data collection, data analysis and reviewing of the manuscript. BS: experimental design, intellectual analysis and reviewing of the manuscript. SG: intellectual analysis and reviewing of the manuscript. AF: intellectual analysis and reviewing of the manuscript. DB: intellectual analysis and reviewing of the manuscript. CP: experimental design, intellectual analysis and reviewing of the manuscript. VH: experimental design, intellectual analysis, writing and reviewing of the manuscript. All authors have read and agreed to the published version of the manuscript.

Conflict of interest

Nothing to declare.

Funding

ASM is supported by an Aspirant fellowship of the Fonds National de la Recherche Scientifique (FNRS), Belgium. CP is a postdoctoral specialist of the FNRS (grant 1.R016.20), Belgium. VH is supported by a clinical post-doctoral mandate of the FNRS

(grant 1R20221F), Belgium. The project was funded by an FRNS project grant (grant T011421F).

Acknowledgements

We thank Caroline Bouzin and Aurélie Daumerie, from the IREC Imaging Platform (2IP), for their valuable help concerning technical aspects of imaging acquisition and quantification.

References

- Bachert C, Marple B, Schlosser RJ, et al. Adult chronic rhinosinusitis. *Nat Rev Dis Primers*. 2020 Dec 1;6(1).
- Rudmik L. Economics of chronic rhinosinusitis. *Curr Allergy Asthma Rep*. 2017 Apr;17(4):20.
- Fokkens WJ, Lund VJ, Hopkins C, et al. European Position Paper on Rhinosinusitis and Nasal Polyps 2020. *Rhinology*. 2020 Feb 20;58(Suppl S29):1-464.
- Newton J. A review of nasal polyposis. *Ther Clin Risk Manag*. 2008 Apr;4:507-12.
- Massoth L, Anderson C, McKinney KA. Asthma and chronic rhinosinusitis: diagnosis and medical management. *Med Sci (Basel)*. 2019 Mar 27;7(4):53.
- Gohy S, Hupin C, Ladjemi MZ, Hox V, Pilette C. Key role of the epithelium in chronic upper airways diseases. *Clin Exp Allergy*. 2020 Feb;50(2):135-146.
- Fujieda S, Imoto Y, Kato Y, et al. *Allergol Int*. 2019 Oct;68(4):403-412.
- Vlaminck S, Acke F, Scadding GK, Lambrecht BN, Gevaert P. Pathophysiological and clinical aspects of chronic rhinosinusitis: current concepts. *Front Allergy*. 2021 Oct 27;2:741788.
- Shin SH, Ye MK, Park J, Geum SY. Immunopathologic role of eosinophils in eosinophilic chronic rhinosinusitis. *Int J Mol Sci*. 2022 Nov 1;23(21):13313.
- van Zele T, Gevaert P, Watelet JB, et al. Staphylococcus aureus colonization and IgE antibody formation to enterotoxins is increased in nasal polyposis. *J Allergy Clin Immunol*. 2004 Oct;114(4):981-3.
- Vickery TW, Ramakrishnan VR, Suh JD. The role of Staphylococcus aureus in patients with chronic sinusitis and nasal polyposis. *Curr Allergy Asthma Rep*. 2019 Mar 11;19(4):21.
- Maniakas A, Asmar MH, Renteria Flores AE, et al. Staphylococcus aureus on sinus culture is associated with recurrence of chronic rhinosinusitis after endoscopic sinus surgery. *Front Cell Infect Microbiol*. 2018 May 15;8:150.
- Ou J, Wang J, Xu Y, et al. Staphylococcus aureus superantigens are associated with chronic rhinosinusitis with nasal polyps: a meta-analysis. *Eur Arch Otorhinolaryngol*. 2014 Oct 1;271(10):2729-36.
- Foreman A, Holtappels G, Psaltis AJ, et al. Adaptive immune responses in Staphylococcus aureus biofilm-associated chronic rhinosinusitis. *Allergy*. 2011 Nov;66(11):1449-56.
- Georas SN, Rezaee F. Epithelial barrier function: at the front line of asthma immunology and allergic airway inflammation. *J Allergy Clin Immunol*. 2014 Sep;134(3):509-20.
- Steeleant B, Seys SF, Boeckstaens G, Akdis CA, Ceuppens JL, Hellings PW. Restoring airway epithelial barrier dysfunction: a new therapeutic challenge in allergic airway disease. *Rhinology*. 2016 Sep 1;54(3):195-205.
- Chegini Z, Didehdar M, Khoshbayan A, Karami J, Yousefimashouf M, Shariati A. The role of Staphylococcus aureus enterotoxin B in chronic rhinosinusitis with nasal polyposis. *Cell Commun Signal*. 2022 Mar 9;20(1):29.
- Marcus S, Roland LT, DelGaudio JM, Wise SK. The relationship between allergy and chronic rhinosinusitis. *Laryngoscope Invest Otolaryngol*. 2019;Feb 20;4(1):13-7.
- Wilson KF, McMains KC, Orlandi RR. The association between allergy and chronic rhinosinusitis with and without nasal polyps: an evidence-based review with recommendations. *Int Forum Allergy Rhinol*. 2014 Feb;4(2):93-103.
- Woodrow JS, Sheats MK, Cooper B, Bayless R. Asthma: the use of animal models and their translational utility. *Cells*. 2023 Apr 5;12(7):1091.
- Takeda K, Gelfand EW. Mouse models of allergic diseases. *Curr Opin Immunol*. 2009 Dec;21(6):660-5.
- Chamanza R, Wright JA. A review of the comparative anatomy, histology, physiology and pathology of the nasal cavity of rats, mice, dogs and non-human primates. relevance to inhalation toxicology and human health risk assessment. *J Comp Pathol*. 2015 Nov;153(4):287-314.
- Kim DW, Khalmuratova R, Hur DG, et al. Staphylococcus aureus enterotoxin B contributes to induction of nasal polypoid lesions in an allergic rhinosinusitis murine model. *Am J Rhinol Allergy*. 2011 Nov;25(6).
- Leite-Santos F, Tamashiro E, de Andrade Batista Murashima A, Anselmo-Lima WT, Valera FCP. Which are the best murine models to study eosinophilic chronic rhinosinusitis? a contemporary review. *Braz J Otorhinolaryngol*. 2023 Sep 15;89(6):101328.
- Gevaert P, Wong K, Millette LA, Carr TF. The role of IgE in upper and lower airway disease: more than just allergy! *Clin Rev Allergy Immunol*. 2022 Feb 18;62(1):200-15.
- Delemarre T, Holtappels G, De Ruyck N, et al. Type 2 inflammation in chronic rhinosinusitis without nasal polyps: another relevant endotype. *J Allergy Clin Immunol*. 2020 Aug;146(2):337-343.e6.
- Shin H. Animal models in CRS and pathophysiological insights gained: a systematic review. *Laryngoscope Invest Otolaryngol*. 2016 Oct 2;1(5):116-23.
- Al-Sayed AA, Agu RU, Massoud E. Models for the study of nasal and sinus physiology in health and disease: a review of the literature. *Laryngoscope Invest Otolaryngol*. 2017 Dec;2(6):398-409.
- Norlander T, Fukami M, Westrin KM, Stiernä P, Carlsöö B. Formation of mucosal polyps in the nasal and maxillary sinus cavities by infection. *Otolaryngol Head Neck Surg*. 1993;Sep 1;109(3):522-9.
- Soyka MB, Wawrzyniak P, Eiwegger T, et al. Defective epithelial barrier in chronic rhinosinusitis: the regulation of tight junctions by IFN- γ and IL-4. *J Allergy Clin Immunol*. 2012 Nov;130(5):1087-1096.e10.
- Huvenne W, Callebaut I, Plantinga M, et al. Staphylococcus aureus enterotoxin B facilitates allergic sensitization in experimental asthma. *Clin Exp Allergy*. 2010 Mar 1;40(7):1079-90.
- Finkelman FD, Wills-Karp M. Usefulness and optimization of mouse models of allergic airway disease. *J Allergy Clin Immunol*. 2008 Mar;121(3):603-6.
- Sahu N, Morales JL, Fowell D, August A. Modeling susceptibility versus resistance in allergic airway disease reveals regulation by tec kinase Itk. *PLoS One*. 2010 Jun 28;5(6):e11348.
- Atochina EN, Beers MF, Tomer Y, et al. Attenuated allergic airway hyperresponsiveness in C57BL/6 mice is associated with enhanced surfactant protein (SP)-D production following allergic sensitization. *Respir Res*. 2003;4(1):15.
- Baroody FM, Mucha SM, deTineo M, Naclerio RM. Nasal challenge with allergen leads to maxillary sinus inflammation. *J Allergy Clin Immunol*. 2008 May;121(5):1126-1132.e7.
- Helman SN, Barrow E, Edwards T, DelGaudio JM, Levy JM, Wise SK. The role of allergic rhinitis in chronic rhinosinusitis. *Immunol Allergy Clin North Am*. 2020 May;40(2):201-14.
- Hamizan AW, Loftus PA, Alvarado R, et al. Allergic phenotype of chronic rhinosinusitis based on radiologic pattern of disease. *Laryngoscope*. 2018 Sep;128(9):2015-21.
- Baral E, Vánky F. Effect of tamoxifen on cell-mediated auto-tumor lysis. *J Clin Lab Immunol*. 1987 Feb;22(2):97-100.
- Ryu G, Bae JS, Kim JH, et al. Role of IL-17A in chronic rhinosinusitis with nasal polyp. *Allergy Asthma Immunol Res*. 2020 May;12(3):507-22.
- Lee M, Park CG, Huh BK, et al. Sinonasal

- delivery of resveratrol via mucoadhesive nanostructured microparticles in a nasal polyp mouse model. *Sci Rep.* 2017 Jan 10;7:40249.
41. Kim DY, Lee SH, Carter RG, Kato A, Schleimer RP, Cho SH. A recently established murine model of nasal polyps demonstrates activation of B cells, as occurs in human nasal polyps. *Am J Respir Cell Mol Biol.* 2016 Aug;55(2):170–5.
 42. Jin J, Rha KS, Kim DW, Kim YM. IL-17C expression in nasal epithelial cells of chronic rhinosinusitis with nasal polypsis. *Eur Arch Otorhinolaryngol.* 2014 May;271(5):1097–105.
 43. Choi MR, Xu J, Lee S, et al. Chloroquine treatment suppresses mucosal inflammation in a mouse model of eosinophilic chronic rhinosinusitis. *Allergy Asthma Immunol Res.* 2020 Nov;12(6):994–1011.
 44. Wee JH, Ko YK, Khalmuratova R, Shin HW, Kim DW, Rhee CS. Effect of lipopolysaccharide and polyinosinic:polycytidylic acid in a murine model of nasal polyp. *Sci Rep.* 2021 Jan 13;11(1):1021.
 45. Wu L, Rodríguez-Rodríguez C, Cun D, Yang M, Saatchi K, Häfeli UO. Quantitative comparison of three widely-used pulmonary administration methods in vivo with radiolabeled inhalable nanoparticles. *Eur J Pharm Biopharm.* 2020 Jul;152:108–115.
 46. Southam DS, Dolovich M, O'Byrne PM, Inman MD. Distribution of intranasal instillations in mice: effects of volume, time, body position, and anesthesia. *Am J Physiol Lung Cell Mol Physiol.* 2002 Apr;282(4):L833–9.
 47. Yii ACA, Tay TR., Choo XN, Koh MSY, Tee AKH, Wang DY. Precision medicine in united airways disease: a “treatable traits” approach. *Allergy.* 2018 Oct 10;73(10):1964–78.
 48. Bankhead P, Loughrey MB, Fernández JA, et al. QuPath: open source software for digital pathology image analysis. *Sci Rep.* 2017 Dec 1;7(1).
 49. Marée R, Rollus L, Stévans B, et al. Collaborative analysis of multi-gigapixel imaging data using Cytomine. *Bioinformatics.* 2016 May 1;32(9):1395–401.
 50. Courtoy GE, Leclercq I, Froidure A, Schiano G, Morelle J, Devuyst O, et al. Digital image analysis of picosirius red staining: a robust method for multi-organ fibrosis quantification and characterization. *Biomolecules.* 2020 Nov 22;10(11):1585.

Valérie Hox

Department of Otorhinolaryngology
Cliniques Universitaires Saint-Luc
and pole of Pneumology, ORL (airways)
et Dermatology (skin) (LUNS)

Institute of Experimental and Clinical
Research
UCLouvain
1200 Brussels
Belgium

E-mail: Valerie.hox@uclouvain.be

Alba Sánchez-Montalvo^{1,2}, Marylène Lecocq¹, Elise Bouillet¹, Brecht Steelant²,
Sophie Gohy^{1,3,4}, Antoine Froidure^{1,3}, Dominique Bullens^{2,5}, Charles Pilette^{1,3},
Valérie Hox^{1,6}

Rhinology 62: 4, 446 - 456, 2024

<https://doi.org/10.4193/Rhin23.331>

Received for publication:

September 4, 2023

Accepted: February 19, 2023

Associate Editor:

Ahmad Sedaghat

¹ Pole of Pneumology, ORL (airways) and Dermatology (skin) (LUNS), Institute of Experimental and Clinical Research (IREC), Université Catholique de Louvain (UCLouvain), Brussels, Belgium

² Department of Microbiology, Immunology and Transplantation, Allergy and Clinical Immunology Research Group, KULeuven, Leuven, Belgium

³ Department of Pneumology, Cliniques Universitaires Saint-Luc, Brussels, Belgium

⁴ Cystic Fibrosis Reference Centre, Cliniques Universitaires Saint-Luc, Brussels, Belgium

⁵ Clinical Division of Paediatrics, UZ Leuven, Leuven, Belgium

⁶ Department of Otorhinolaryngology, Cliniques Universitaires Saint-Luc, Brussels, Belgium

This manuscript contains online supplementary material

SUPPLEMENTARY MATERIAL

Materials and methods

Mouse model of eCRS

Animal model

7-8 weeks old C57BL/6NRJ female mice (weighting 20-25g) were purchased from the Janvier Labs (Centre d'élevage Roger Janvier) facility. Mice were housed in an animal facility with agreement reference LA1230292, maintained at 22-25°C and 50-60% relative humidity. A summary of the experimental protocol is shown in Figure 1. Mice were randomly divided into four different groups with $n = 4$ to 10/group: control, SEB, OVA, and OVA+SEB. Briefly, based on Kim et al. 2011, ovalbumin (OVA) was used to sensitize mice with an intraperitoneal (i.p.) injection of a total volume of 200 μ l containing 25 μ g of OVA in 2 mg of aluminum hydroxide gel on days 0 and 7. Control mice were injected with 200 μ l of Phosphate-Buffered Saline (PBS). This was followed by daily intranasal (i.n.) challenges from day 14 to 20 with 6% OVA diluted in 20 μ l of PBS. Mice in the control and SEB groups received i.n. challenges with PBS instead. These i.n. challenges were continued at a rate of three times a week for 8 consecutive weeks. Mice that were planned to develop an eCRS, received, in addition to these i.n. OVA-challenges, a second i.n. challenge with 10 ng of SEB diluted in 20 μ l of PBS, also three times a week for eight weeks. For i.n. installations, mice were slightly sedated by using isoflurane inhalation (Isoflutek 1,000 mg/g, Karizoo Laboratories). After i.n. installations, each mouse was closely followed until completely awakened. All animal experiments were performed in compliance with the ethical committee guidelines and approved under the reference code 2018/UCL/MD/42.

Sacrifice and sampling

3 days after the final i.n. challenge, Mice were euthanized by administering an i.p injection of pentobarbital (200mg/kg). First, blood was drawn from the inferior cava vein and centrifuged at 650g for 20 minutes at room temperature (RT) and serum was collected and stored at -20°C for further processing. Nasal lavage (NL) fluid was collected and recovered via the nostrils by softly flushing 1ml of saline solution (NaCl 0.9%) by inserting a 22G cannula (Versatus™ I.V Catheter) through a tracheotomy. Then, the NL was centrifuged at 450g for 5 minutes at 4°C to collect the cell pellet, which was used for performing cytopspins, and the supernatant was stored at -20°C for further processing. Bronchoalveolar Lavage (BAL) was collected by inserting a second catheter via the created tracheotomy, through which 1mL of saline solution was gently flushed and recovered from the bronchioles⁽⁵⁰⁾. Like the NL, the BAL was centrifuged at 450g for 5 minutes at 4°C to collect the cell pellet, which was used for performing cytopspins, and the supernatant was stored at -20°C for further processing. Then, an intracardiac perfusion was

performed with 5 ml of saline solution to rinse the lung blood vessels and then the lungs were fixed in formaldehyde 4% for further histology analysis. Skulls were harvested and skin and soft tissues, as well as the inferior mandibula, were removed. They were fixed in formaldehyde 4% and decalcified in 20 ml of Osteoral™ (RAL Diagnostics) for 5 days. After decalcification, the snout and brain were removed to keep the skull region of interest containing the paranasal sinuses. The decalcified skull and lungs were dehydrated and treated according to standard paraffin-embedding procedures. Paraffinized Skulls and lungs were cut into 4 μ m sections by using a semi-automated microtome (ThermoFisher Scientific).

Cytopspins for inflammatory cell count

NL and BAL were collected as described and centrifuged at 450g for 5 minutes at 4°C to separate the cell pellet. The supernatant was stored, and cells were counted by using a TC20™ Automated Cell Counter (Bio-Rad). Cells were loaded into a Thermo Shandon Cytospin Centrifuge (Thermo Shandon) following the manufacturer's instructions and centrifuged at 500 revolutions per minute (rpm) for 5 min. Cytopspins were stained by using the Kwik-Diff™ kit (Thermo Fisher Scientific). In brief, sections are fixed in the 'Kwik-Diff' fixative solution I. Then the slides are stained with the 'Kwik-diff' eosin solution II and followed by a counterstaining with the 'Kwik-diff' methylene blue solution III. Last, slides are rinsed in distilled water to remove excess stain, coverslipped, and scanned by using a Panoramic scan II (3DHitech).

Histopathologic analysis of the paranasal sinus epithelium

To analyze the below-mentioned parameters among the different mice groups, we decided to focus on the three fixed areas of both the right and the left maxillary sinus (two areas on the lateral side and one area on the medial side) were taken to evaluate histological features (Figure 2). After being stained by the respective staining protocols, all slides were coverslipped and scanned by using a Panoramic scan II (3DHitech).

To study the epithelial integrity, formation of nasal polyp (NP)-like lesions and epithelial thickness, H&E staining was performed. Briefly, paraffinized 4 μ m sections the sections underwent deparaffination and rehydration by putting them into toluene and methanol for 3 times 5 minutes for each solvent and then, in tap water and distilled water for 5 minutes each. Next, the slides were incubated into hematoxylin for 5 minutes and after that, they were rinsed in tap and distilled water for 5 minutes each. Further, the slides were incubated with eosin for 10 minutes, followed by a double wash in methanol and a final incubation

in xylene for 3 times 5 minutes each. Finally, the slides were coverslipped and scanned by using a Panoramic scan II (3DHitech). To count NP-like lesions per mouse, consecutive sections at three consecutive levels of the skull were evaluated, similar to the initial model published by Kim ⁽²⁰⁾. NP-like lesions were defined as a projection from the lining of the epithelium to the lumen, with a tear-drop shape and filled with eosinophils. NP-like lesions were only considered when found in three consecutive sections at three different levels in the skull to account for artefacts.

To evaluate epithelial thickness, the cellular space between the basolateral to the apical pole of the epithelial cell layer, was manually measured by using Cytomine ⁽⁴⁵⁾.

To evaluate basement membrane thickness, the space between the basolateral pole of the epithelial layer and the first layer of submucosal glands was manually measured by using Cytomine ⁽⁴⁵⁾.

Giemsa staining was performed to evaluate goblet cell hyperplasia and eosinophilic infiltration. Quantification was performed by using QuPath ⁽⁴⁴⁾ and expressed as a percentage of positive area. Giemsa staining was performed to evaluate goblet cell hyperplasia and eosinophilic infiltration. Briefly, paraffinized 4 µm sections underwent deparaffination and rehydration by putting them into toluene and methanol for 3 times 5 minutes for each solvent and then, in tap water and distilled water for 5 minutes each. Next, the slides were incubated with Giemsa solution (Merck) 2% for 20 minutes. Then, they were differentiated with absolute ethanol, coverslipped and scanned by using a Panoramic scan II (3DHitech).

Sirius red (SR) staining was performed to evaluate collagen deposition. Briefly, paraffinized 4 µm sections underwent deparaffination and rehydration by putting them into toluene and methanol for 3 times 5 minutes for each solvent and then, in tap water and distilled water for 5 minutes each. Next, the slides were permeabilized by incubating them with phosphomolybdic acid for 2 minutes and then were rinsed in tap and distilled water for 5 minutes each. Further, the slides were incubated with Picrosirius Red for 2 hours at room temperature (RT) in a humid chamber. After that, the slides were incubated in hydrochloric acid for 2 minutes in light agitation, followed by a wash in distilled water and dehydration in absolute ethanol and a final incubation in xylene for 3 times 5 minutes each. Finally, the slides were coverslipped and scanned by using a Panoramic scan II (3DHitech). Quantification was performed by using ImageJ, as described by Courtoy et al. ⁽⁴⁶⁾, and expressed as a percentage of positive stained area following the formula:

$$\% \text{ positive staining} = \frac{\text{Positive area}}{\text{Total area}} \times 100$$

Histopathologic analysis of the bronchial epithelium

Giemsa staining was also performed in paraffinized 4 µm sections of the fixed left as described above to evaluate the general state of the lung epithelium and to evaluate eosinophilic infiltration. Slides were coverslipped and scanned by using a Panoramic scan II (3DHitech).

Immunohistochemical expression of tight junctions in the sinus epithelium

Paraffinized 4 µm sections were deparaffinized in toluene and rehydrated through graded series from methanol to distilled water. Sections underwent antigen retrieval treatment using an antigen retriever (2100 antigen retriever, Aptum Biologics). Endogenous peroxidase and non-specific protein binding sites were inactivated by incubation in Bloxall (Vector Laboratories, Inc., USA) for 15 min and with 0.3% hydrogen peroxide in tris-buffered saline (TBS) 5% goat serum (Abcam) for 30 min. As primary antibodies, rabbit anti-mouse Claudin 3 (Invitrogen, 34-1700), mouse anti-mouse Claudin 4 (Invitrogen, 32-9400), rabbit anti-mouse occludin (Invitrogen, 71-1500) and mouse anti-ZO1 (Invitrogen, 33-9100) were respectively incubated overnight at 4°C. After washing with TBS 0.1% Tween 20 (TBS-T), sections were incubated with either goat anti-rabbit poly HRP (B40962, ThermoFisher) or goat anti-mouse poly HRP (B40961, ThermoFisher) as secondary antibody for 40 minutes. Revelation was performed by using a DAB Plus Substrate Kit (D4168, Sigma-Aldrich) according to the manufacturer's instructions. Sections were counterstained with Hematoxylin (Sigma-Aldrich) and coverslipped. Slides were scanned using a Panoramic scan II (3DHitech). Quantification was performed by using QuPath ⁽⁴⁴⁾ and expressed as percentage of positive area. To compare the above-mentioned parameters between the different mice groups, three areas of both the right and the left maxillary sinus (two areas on the lateral side and one area on the medial side) were taken to evaluate histological features (Figure 2).

Total IgE measurement

Serum and NL levels of total IgE were determined by sandwich ELISA. Briefly, a 96-well microplate (Greiner Bio-one) was coated with purified mouse IgE (BD Pharmingen 553413) as capture antibody and was incubated overnight at 4°C. Next, the plates were blocked with bovine serum albumin (BSA) 1% and incubated for 1h at 37°C and washed with PBS + 0.05% Tween 20. Standards (BD Pharmingen, 557079) and samples were added to the plates and incubated for 2h at 37°C. After washing, the detection was performed with biotinylated anti-mouse IgE (BD Pharmingen, 553419) for 1h at 37°C, followed by Streptavidin-

HRP amplification for 30 min at room temperature. Revelation was performed using 1-Step™ Ultra TMB (Thermo Fisher Scientific) and sulfuric acid was added to stop the reaction. The absorbance was measured at 405 nm on a microplate reader (iMark™ Microplate Absorbance Reader, Bio-Rad Laboratories, Inc). The lower limit of detection was 2.87 ng/ml. Serum samples were diluted 1:25 in PBS and NL samples were used undiluted.

Statistical analysis

Analysis was performed with GraphPad Prism version 8.0.0 (GraphPad Software, San Diego, CA, USA). Results are presented as median from each group ± interquartile range (IQR). Statistical differences between experimental groups were evaluated using the Kruskal-Wallis test for comparing multiple groups. A value of $p < 0.05$ was considered significant.

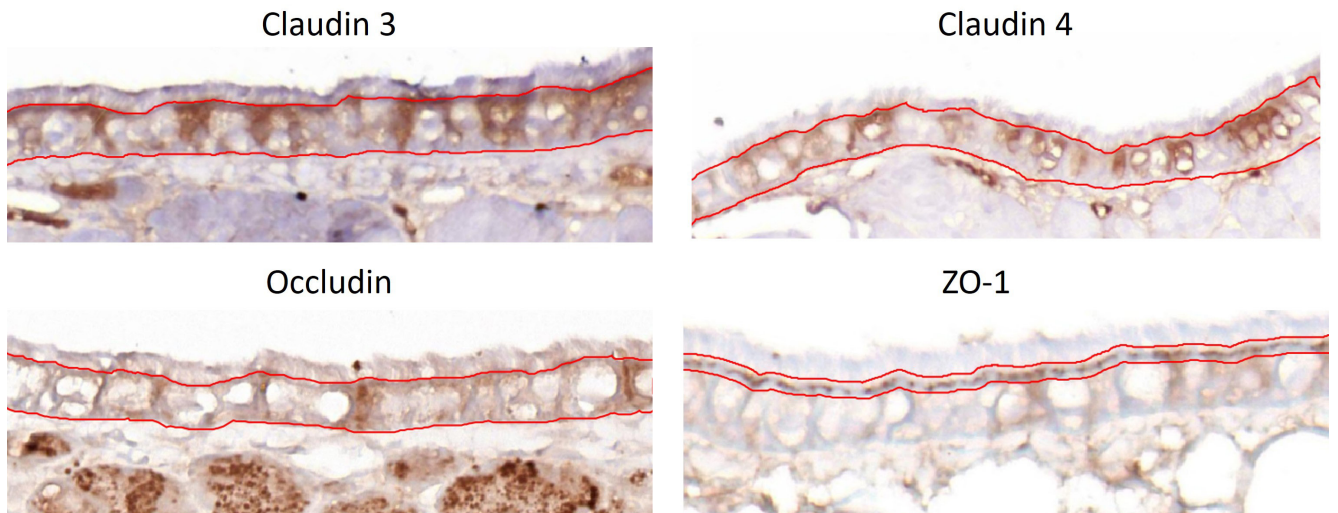


Figure S1. Validation and quantification strategy for tight junctions staining. In red, the region of interest considered for the quantification.

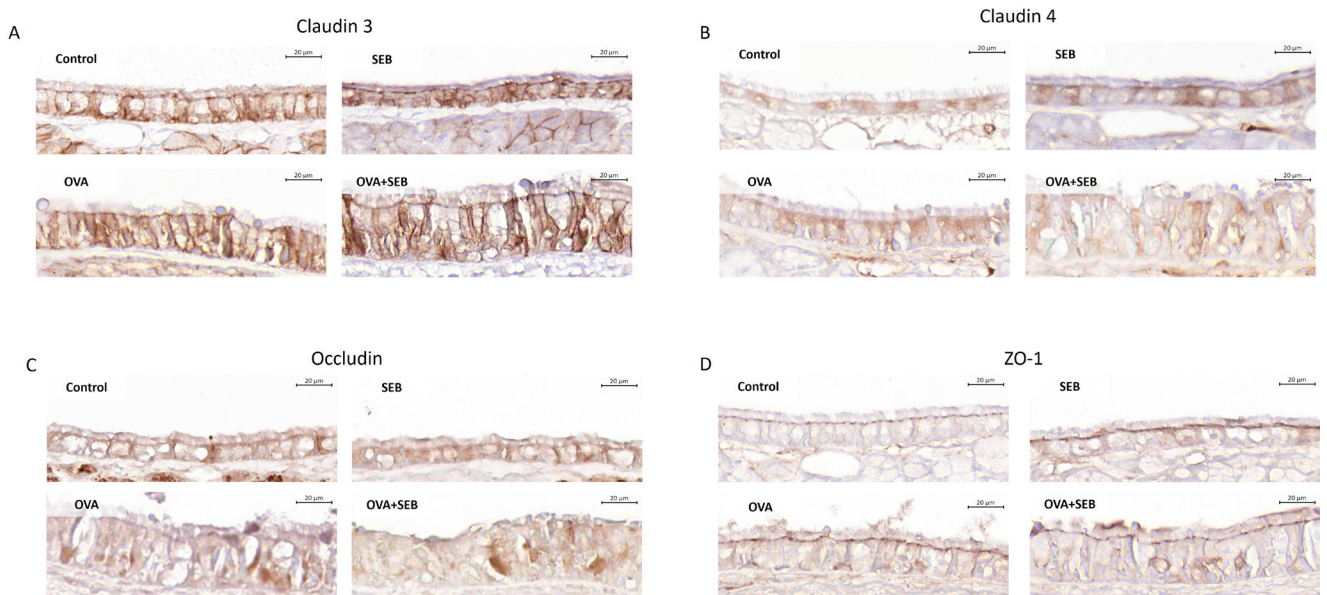


Figure S2. Tight junctions' expression in experimental eCRS. Representative sections of the epithelial layer from maxillary sinuses. A) Claudin 3 staining. B) Claudin 4 staining. C) Occludin staining. D) ZO-1 staining. Scale bar= 20 μm.